Transient Motions and Static Poses in Soft, Viscous-Driven Actuators

Rafael Gottlieb[1], Atilla Osan[1], Mattieu Zhai[1], Yoav Matia[2], and Kirstin Petersen[3]

***Abstract*— In this paper we further studies of viscous-driven fluidic elastomer actuators. Specifically, the one we investigate consists of simple elastomer bellows connected in series by slender tubes and arranged in two columns around a neutral plane. The slender tubes and wide bellows configuration result in advective-diffusive flow, which causes non-uniform pressure distributions throughout the actuator and, as a consequence, complex transient 2D deformations that depends only on the shape of the input pressure profile, rather than multiple pressure sources and/or valves. We extend upon previous work by demonstrating a three-finger 'manipulator' capable of stabilizing a computer mouse and operating its scroll wheel. This demonstration illustrates the interplay between input pressure gradients and motion output, and additionally how a single valve can further enable stationary poses throughout the workspace of the actuator. This type of embodied control matches well the infinite passive degrees of freedom afforded by the soft material, and holds great promise for future applications in soft robotics.**

I. INTRODUCTION

Fluid elastomer actuators (FEAs) continue to be the hallmark of soft robotics, combining simple and inexpensive mechanical design and fabrication with intuitive control and large deformations [1]. While these actuators are prized for their infinite passive degrees of freedom, the price, volume, and weight of the drive mechanism scales poorly with the number and complexity of deformations needed. To address this challenge, we recently introduced a new method by which FEAs can achieve complex transient deformation patterns using just a single pressure inlet [2]. Typical FEAs are driven by spatially uniform pressure distributions. In contrast, the simple actuators used in this paper rely on two columns of elastomer bellows arranged around a neutral axis, connected in series by thin tubes that causes viscous flow and therefore nonuniform pressure distributions which, in turn, lead to temporary deformation beyond the neutral axis (Fig. 1A). As part of this recent work, we introduced a predictive model, described and demonstrated five governing mechanisms, and showed their use in a six-legged, untethered walking robot.

In this paper, we expand on the methods for such viscous-driven actuators by incorporating a single valve, such that our system can exhibit both transient and steady-state deformations, and demonstrate its use case in a three-finger manipulator operating the scroll wheel on a computer mouse. To inform their use in future mobile robots, we further elaborate on how the input pressure gradients affect the motion of the actuator. This design methodology has the potential to drastically enhance the capabilities of soft robots, by alleviating controller complexity and instead exploiting embodied intelligence in the form of material-fluid interactions.

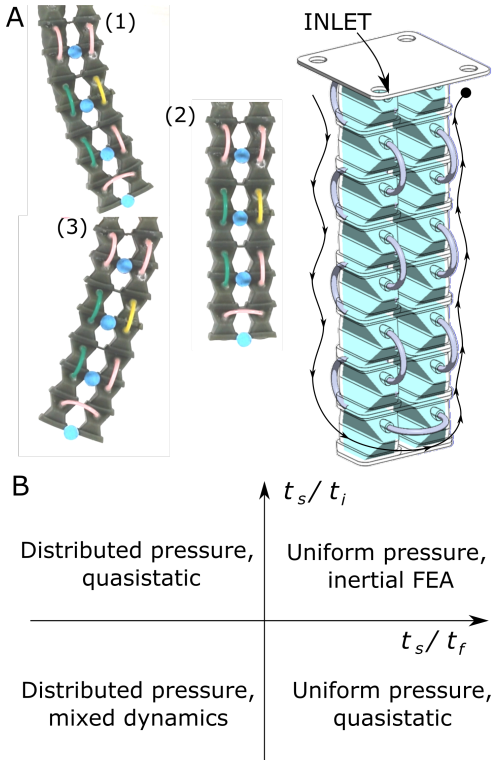

Fig. 1: A) Concept behind viscous-driven actuators. (1-3) shows a sequence of video frames. In (1) a steep positive pressure gradient is applied to the actuator causing the bellows closer to the inlet expand before the rest due to viscous resistance in the tubes, in turn causing the entire actuator to bend right. In (2) the pressure has equalized throughout the bellows, and the actuator is extended. In (3) a steep negative pressure gradient is applied to the inlet causing the actuator to momentarily bend to the left. B) FEA designs plotted as a function of the ratios between solid-to-input transients and solid-to-fluid timescales.

This work was supported by a Packard Fellowship for Science and Engineering and NSF award #2042411.

[1]Sibley School of Mechanical and Aerospace Engineering, Cornell University, Ithaca, NY 14853, USA. rdg244@cornell.edu, ado27@cornell.edu, mz375@cornell.edu. The first three authors contributed equally to this work. [2] Department of Mechanical Engineering, Ben-Gurion University of the Negev, Be'er Sheva, 8410501, Israel. yoavmatia@bgu.ac.il. [3]School of Electrical and Computer Engineering, Cornell University, Ithaca, NY 14853, USA. kirstin@cornell.edu

II. BACKGROUND AND RELATED WORK

The key to viscous-driven FEAs is a balance between the three governing time scales: the elastic-inertial timescale of the solid, t_s, the viscous-elastic timescale of the fluid, t_f, and the timescale of the input transients, t_i. When considering the design space characterized by the ratios of the solid-to-input timescale, t_s/t_i, and the solid-to-fluid timescale, t_s/t_f, we find four actuation regimes (Fig. 1B).

"Classic FEAs" exist in the fourth quadrant. The timescale of the input is slow relative to the solid response ($t_s/t_i \ll 1$), and the solid, in turn, is slower than the fluid timescale ($t_s/t_f \gg 1$). Such actuation methods, e.g. [3], [4], [5], couple spatially uniform pressure distribution with quasistatic transient behavior. With a single inlet, these actuators can only expand and contract, or follow a prescribed curvature depending on pre-patterned strain layers.

Combustion-driven and dynamic-response FEAs are similar, [6], [7], but the solid is too slow to track the input and fluid transients quasistatically ($t_s/t_i \gg 1$). These actuators couple uniform pressure distribution ($t_s/t_f \gg 1$) with solid inertial response.

Recent work, mostly theoretical, showed how viscous fluids can also be used to produce transient, damped spatial motion patterns with single inlet FEAs [8], [9], [10]. These types of actuators are characterized by nonuniform spatial pressure distribution ($t_s/t_f \ll 1$) with short input transients and quasistatic behavior ($t_s/t_i \gg 1$).

The new insight of [2] came from designing actuators that operate in a regime where time scales are of comparable magnitudes ($t_s/t_f = O(1)$, $t_s/t_i = O(1)$) to one (or more) orders-of-magnitude apart ($t_s/t_f = o(1)$, $t_s/t_i = o(1)$); where deformations can be driven by spatial and temporal viscous pressure variations generated by temporal inlet pressure gradients.

The concept is shown in Fig. 1A; in its simplest possible configuration, a closed series of hollow elastomer bellows are arranged in two columns around a neutral axis and interconnected in series starting from the top left, down through the left column, over to the right, and back up, ending in the top right bellow (the actuator has no outlet). By using slender flexible tubes to connect the bellows, the flow between the bellows acts viscous, which in turn causes nonuniform pressure distributions and nonuniform spatial deformations.

For example, as shown in Fig. 1(1), when a steep positive pressure gradient is applied to the inlet, the top left bellows inflate and expand faster than the subsequent bellows, and the actuator bends towards the right. Eventually, the pressure evens out and the actuator converges to an expanded state along the neutral axis (Fig. 1(2)). Now if a negative pressure is applied to the inlet, the top left bellows deflate and contract before the bellows in the right column and the actuator bends to the left, before eventually settling on a contracted pose along the neutral axis (Fig. 1(3)). In this manner, varying the frequency, amplitude, and duty cycle of the inlet pressure can produce complex deformations across space and time with just a single inlet driven by a syringe pump or similar.

Note that while conceptually, this is similar to the methods used in [4], where different segments of a robot composed of FEAs were driven from a single pressure inlet sourced through varying length tubes. The major difference however is that to achieve complex spatio-temporal motion, our controller is embedded within the elastomer structure of the actuator to produce a compact solution. In the original work, we further introduced a predictive model of the actuator deformation consisting of two governing equations that related 1) the change in fluid flux with the unsteady pressure term and the change in fluid cross-section due to the resultant from the solid domain, and 2) the linear inertia, the curvilinear tangential and normal force, and the rotary inertia. For lack of space, we refer the reader to study the details of this model in [2].

While the viscous-elastic to inertial elastic timescale ratio is critical to define the regime in which the FEA operates, the viscous-elastic to input timescale ratios are the easiest to modulate to change the behavior of the actuator. In this paper, we demonstrate of a three-finger manipulator operating a computer mouse. We chose this demo to serve multiple purposes:

- *Scroll action:* Iterating the main advantage of viscous-driven actuators, we devise an asymmetric cyclical motion capable of a forward 'scroll'.
- *Clicking action:* Illustrating the importance of the solid-input time scale ratio, we pressurize the actuator slowly to produce motion along the neutral axis prompting a scroll-wheel 'click'.
- *Pinch grip:* To keep the mouse steady, we utilize a single valve added in line with the series-connected bellows to achieve stationary poses off the neutral plane of the actuator.
- *Generality:* These actuators can be used for a multitude of tasks, from legged robots as illustrated in [2] to robot manipulators.

III. ELECTRO-MECHANICAL DESIGN

Our 'manipulator' is composed of a scaffold, printed in PLA on a Prusa mkII 3D printer, onto which the three FEAs are mounted such that two can perform a pinch grip on the computer mouse, and the third can reach the scroll wheel. The entire setup is shown in Fig. 2.

Like in the original paper, we worked with actuators composed of 16 elastomer bellows arranged in two columns across a neutral axis. The bellows were printed in two parts (main bellow and lid) on a Carbon 3D printer using SIL-30. The lids were bonded on the bellows afterwards using uncured SIL-30 and baked in an oven for 8hrs at 120^{o}C. The interconnecting tubes were made from ∼30mm long silicone wire (22AWG) in which the copper strands were removed. These tubes were glued to each bellow using Loctite 404 instant adhesive. The actuator's inlet is connected to 3/32" soft PVC Tygon tubing using a 3/32" hose barb luer lock, and through these to a custom built 100mL syringe pump. For data recording purposes, we also mounted an absolute

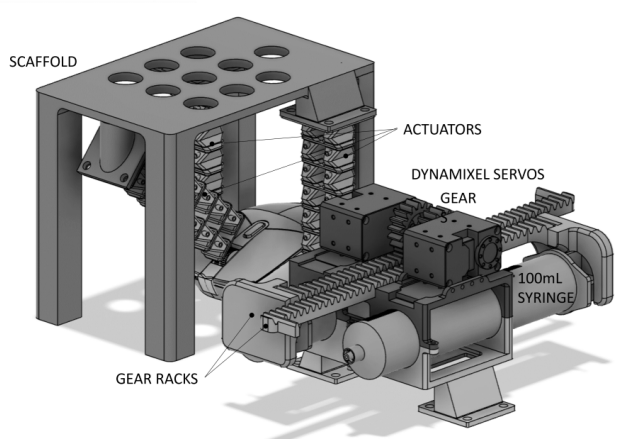

Fig. 2: Assembly of FEA 'manipulator' and syringe pumps.

air pressure sensor with a 20-400kPa range (Phidgets 1140) close to the actuator inlet.

The FEA used to operate the mouse wheel was mounted diagonally as shown in Fig. 2; the two FEAs used to stabilize the mouse were hanging straight down and differed by having an Uxcell miniature solenoid valve inserted in line with the tube connecting the two lower bellows on either side of the neutral axis.

To operate each FEA and the corresponding syringe pump, we used a gear rack and pinion system (18 teeth, pitch diameter 29.6mm) driven by a Dynamixel servos XM430-W350-T. These servos were controlled by a Dynamixel Shield hooked up to an Arduino Due. The two valves were similarly connected to the Arduino Due through an N-channel MOSfet circuit. It is worth noting that the servos used in this paper were an upgrade from those used in the original work and comes with position/torque control which is helpful to achieve accurate pressure cycles. Where the original design was optimized for untethered operation as is critical for mobile robots, we simplified the setup in this paper to be driven by a desktop power supply.

For motion tracking, we recorded the setup using an iPhone 13 set to 1280×720 pixel resolution and 29.99fps, and used a custom Matlab script to track the colored marker located at the tip of the actuator.

IV. FAST MOTIONS

When we add steep pressure gradients to the viscous-driven FEA inlet, the variations in pressure throughout the actuator become more extreme and the tip of the actuator moves further beyond the neutral axis. In the context of the design space graph shown in Fig. 1B, we are essentially moving our system towards a higher ratio of solid to input time scales ($t_s/t_i < 1$). Aided by the predictive model introduced in [2], we designed a forward scroll motion in which we first apply a steep positive pressure gradient to curve the leg, then slowly return the pressure back to ambient. For reference, as described in [2], the elastic inertial timescale of the solid material in this actuator is $t_s = 0.029$.

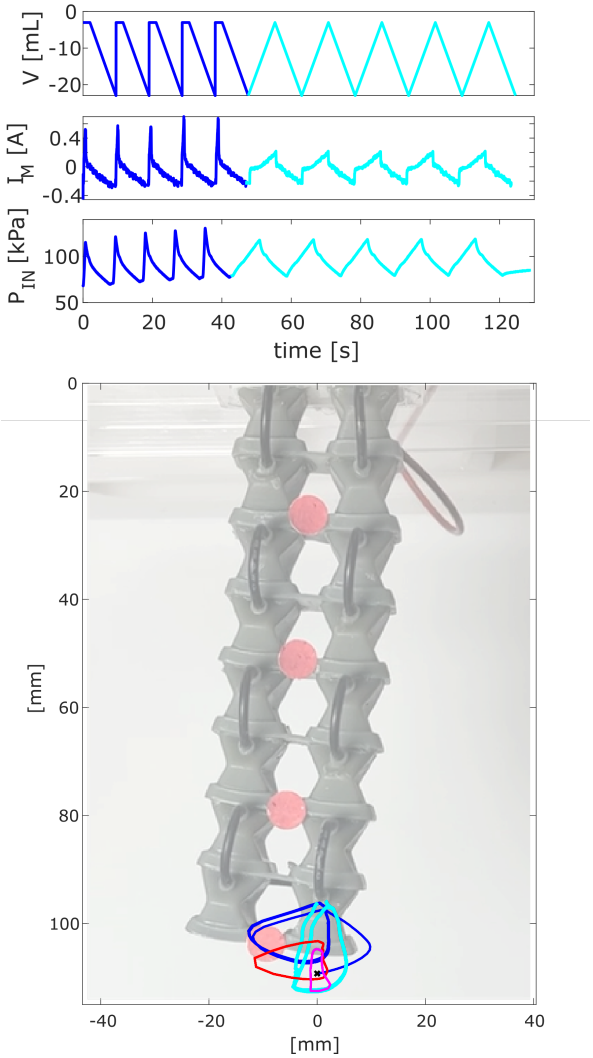

Fig. 3: Recorded and modeled scroll and click operation by a viscous-driven FEA. The top three graphs shows the volume setting for the input to the syringe pump V, the corresponding motor current I_M, and the pressure measured at the inlet of the actuator P_{IN} over time, starting from the first scroll motion cycle. The bottom graph shows the tracked (blue/cyan) and modeled (red/magenta) motion of the actuator tip. The blue and red curves correspond to the scroll motion; the cyan and magenta curves correspond to the click motion. Each cycle is repeated 5 times. The inlet of this actuator is located at the top of the right column.

Here, the fast part of our inlet pressure curve last $t_i = 0.64s$, providing a ratio of $t_s/t_i = 0.045$.

The results are shown in Figure 3. These results were obtained by mounting the actuator vertically and letting it move unrestricted to demonstrate the consistency between the predicted and actual motion. Using the model, we did not account for the varying external contact forces, like those generated by physically contacting a mouse wheel. Therefore, the exact inlet pressure cycle was tuned through an iterative process between the model incorporated into a

COMSOL simulation, the tracked path of the free-hanging actuator, and tracked path of the actuator while in contact with the scroll wheel.

The dark red curve shows the predicted scroll motion, and the dark blue curve shows the tracked path in a recording of the real actuator. To compare these, we used the actual pressure measured at the inlet of the real actuator to inform our simulation. The actuator starts at a negative pressure relative to ambient, causing the leg to compress slightly. The motion cycle starts by adding a step input to the motor position control and consequently the syringe, which causes a steep current draw. In turn, this causes the inlet pressure to increase and the actuator tip to move in a rapid curve to the right. Next, the position of the motor is slowly reset, causing a slower rate of negative motor current, and a slow negative pressure change at the inlet. In turn this produces a slow, almost vertical retraction of the tip.

As expected, we see a similar profile in the real leg. Note that for clarity, we included the brief part of the tracked path that leads the actuator tip from ambient pressure to the beginning of the first scroll cycle. Note also, that the actuator very consistently follows the same path over five repeated cycles. Small discrepancies with the model are seen in both a 13% offset in the y-direction and a slight underestimation of the actual size of the tip motion cycle. We hypothesize that this could be caused by a combination of scaling and offset errors in the pressure sensor.

V. SLOW MOTIONS

With slower pressure gradients at the viscous-driven FEA inlet, the variations in pressure throughout the actuator become less extreme and the tip of the actuator remains closer to the neutral axis. In the context of the design space graph shown in Fig. 1B, we are essentially moving our system towards a lower ratio of solid to input time scales ($t_s/t_i \ll 1$). We designed a 'click' operation using this regime, with an input transient timescale of $t_i = 7.81s$, resulting in a ratio of $t_s/t_i = 0.0037$. Similar to before, we designed this motion by iterating back and forth between the COMSOL simulation, the unrestricted actuator, and the actuator in contact with the scroll wheel.

The predicted and measured results are shown in Fig. 3 in light red (pink) and light blue (cyan), respectively. Again, we find that the model qualitatively predicts the motion cycle of the actuator tip and that the model slightly over-predicts the absolute extension while under-predicting the size of the relative motion cycle. Interestingly, the discrepancy between the model and the real 'click' motion cycle is more pronounced (∼50%) than with the 'scroll' indicating that the model accuracy increases with faster transients. Similar to before, we see good consistency of the path over five consecutive motion cycles.

VI. FREQUENCY RESPONSE

As illustrated by the examples above, the key to the use of viscous-driven, soft actuators is a detailed understanding of the relative time scales. In this section we use the model to do a sinusoidal frequency sweep on the inlet to illustrate how the actuator responds. The results are shown in Fig. 4. At slow frequencies $(50s)^{-1}$, the actuator moves mostly along the neutral (vertical) axis, but as the frequency increases, so does the width of the ellipsoidal path. Note that up to $(11s)^{-1}$ this only prompts a small change in the peak-to-peak vertical extension because of the two columns of bellows which makes it easier to bend the actuator rather than extend it. Note that $(11s)^{-1}$ is approximately similar to the time scale used for the click motion and the slow retraction after the scroll. At higher frequencies $(7.9s)^{-1}$ to $(1.6s)^{-1}$), we see more pronounced horizontal displacement with a slight inclination, and marked decrease in vertical displacement. At the most extreme case $(1.6s)^{-1}$, which is approximately similar to the time scale used for the scroll motion, the

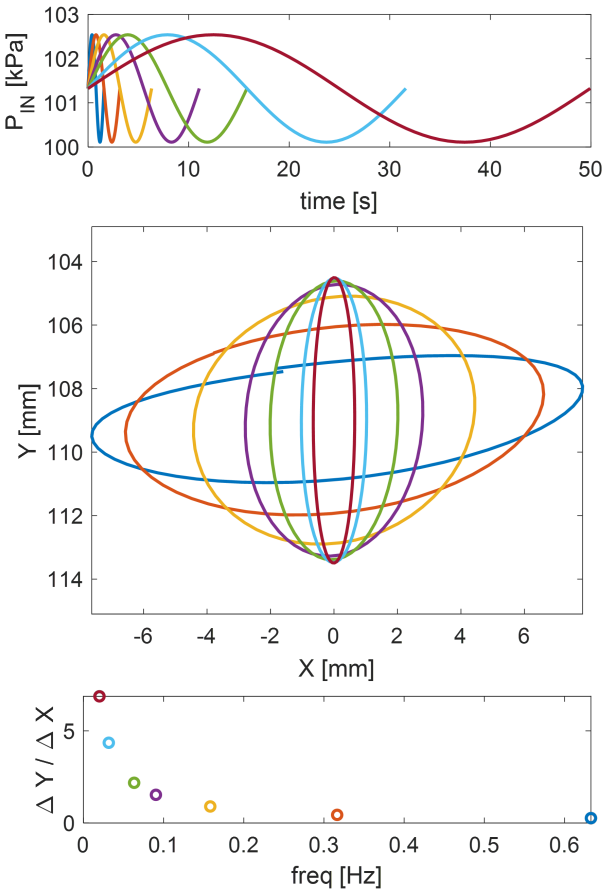

Fig. 4: Simulated actuator frequency response generated in COMSOL. From top to bottom row: Input pressure profile; resulting path generated at the tip of the actuator; ellipsoid shape expressed as the ratio between the maximum difference in horizontal and vertical displacement over a full motion cycle as a function of input frequency. Note that for frequencies up to 0.2Hz, we computed this ratio using X and Y coordinates; but for data points above 0.2Hz, we adjusted for the small incline of the major axis which occurs because the pressure in the actuator no longer has time to equalize before the following cycle begins.

pressure throughout the actuator no longer has time to settle before the following cycle, which is why the tip ends in a position different from the start.

Viewed from a systems lens, it is important to recognize that the steep pressure gradients needed to produce horizontal motions are constrained by the power needed to operate the syringe pump. The Dynamixel servos we use are mid-range motors and relatively strong for their size with a stall torque of 4.1Nm at 12V and a no-load speed of 46rpm. As was shown in Fig. 3, the front stroke we utilized for the scroll motion was the result of a 23mL volume step response, showing a pressure rise time of 0.64s or 35.9mL/s. In addition, the absolute deformation of the actuator is further bounded by the linear elastic region of the elastomer bellows.

VII. STATIONARY POSES

As we have demonstrated above, viscous-driven FEAs are advantageous for generating complex spatio-temporal motions with simple control inputs. However, all motion beyond the neutral axis is necessarily transient, as the pressure eventually equalizes throughout the actuator. Following the minimalist spirit of our design, we show here how adding a single valve at the tip of the actuator, in between the 8th and the 9th bellow allows us to operate it similar to traditional antagonistic FEAs with two inlets.

The results are shown in Figure 5. First, we open the valve, and run a typical pressure cycle (shown in blue). We then close the valve and increase the pressure on the inlet column three times in a row resulting in stationary poses to the left of the neutral axis. As we do so, the actuator tip moves along the red curve, halting at the locations represented by black x's whenever we stop changing the inlet pressure. We repeat this procedure at a higher absolute pressure, then return the actuator to ambient pressure, demonstrate an additional motion cycle (shown in cyan), before repeating the valve experiment with a negative inlet pressure causing stationary poses to the right of the neutral axis.

In the next section, we utilize this design to do a pinch grip on the computer mouse.

VIII. DEMONSTRATION

We combine these experiments into a demonstration in which we use three viscous-driven FEAs to grip and manipulate the wheel of a computer mouse. Fig. 6 shows snapshots from the demonstration video, in which the manipulator successfully grips the mouse, scrolls five times, and then clicks the wheel five times.

Two things are worth noting. First, the actual motion cycle performed by the center FEA differs slightly from that shown in Secs. IV-V due to the fact that it is mounted at an angle and gravity bends it slightly out of axis. Second, when the FEA presses on the scroll wheel, it tends to briefly incur a scroll before the click is induced. To completely avoid this, more accurate tip control may require a smaller FEA, which in turn would affect the maximum pressure gradients needed and the rupture strength of the material.

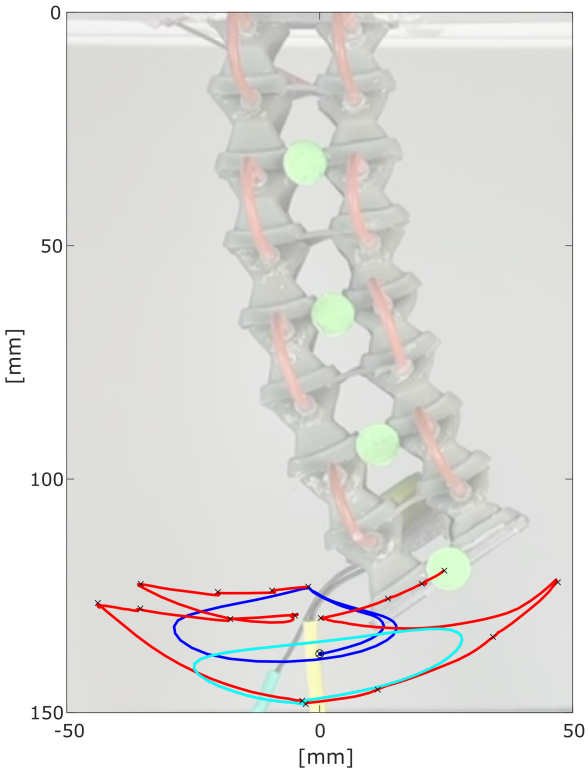

Fig. 5: By adding a valve, the viscous-driven FEAs can be operated in both transient (blue and cyan) and static modes (black x's along the red trajectory). The inlet of this actuator is located at the top of the right column.

IX. SUMMARY AND FUTURE WORK

In this paper, we extended upon past work in viscous-driven FEAs by elaborating on how the timescale of the input pressure profile can affect output motions, and how the addition of a single valve can further permit stationary poses. We demonstrated the use of these in a three-finger manipulator, capable of operating a computer mouse. This diverse utility signifies the importance of this design regime: by leveraging physical control which is embedded within the coupled fluid-elastomer system, we can achieve complex spatio-temporal motion cycles throughout the actuator workspace, using just a single pressure inlet.

In addition to demonstrating the use of these actuators in numerous exciting application areas, from mobile ground- and aqueous robots to more complex manipulators, there are a number of interesting extensions to pursue. To improve the accuracy of predictions, it would be beneficial to incorporate the function of contact forces into the respective predictive model term ($\mathbf{b} = (b_x, b_z)$ used in [2]). Along the same vein, since the solids and the fluids are two-way coupled in this system, it would be exciting to leverage the model and pressure sensors in the actuator for more accurate feedback control. Additionally, we are interested in automated design

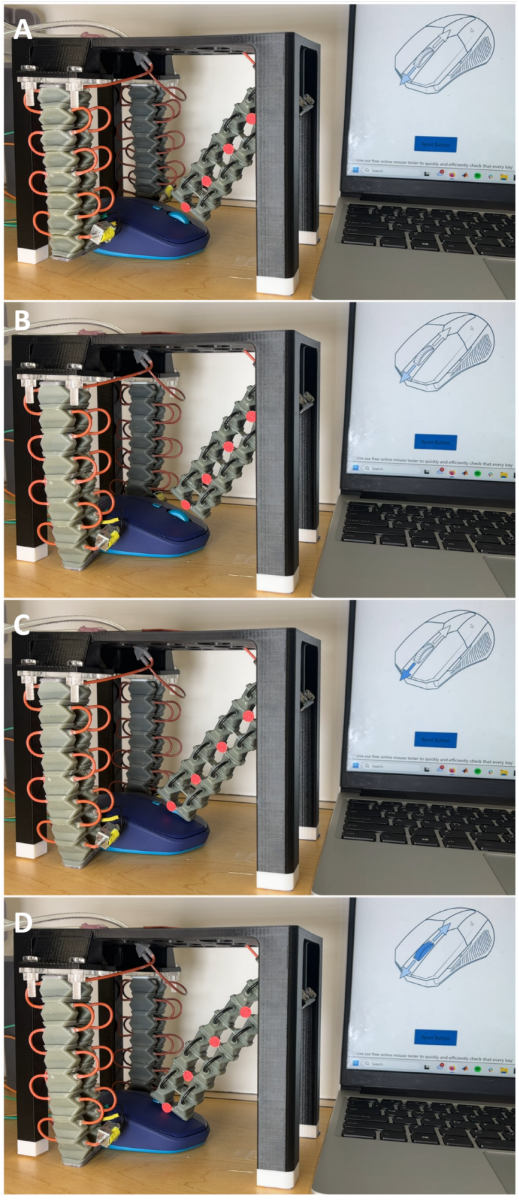

Fig. 6: Still frames from video recording: A) All FEAs are deflated to a negative pressure. B) The valves at the tip of the two FEAs located on either side of the mouse are closed, and next the inlet pressure is increased to produce stationary deformation resulting in a pinch grip. C) The center FEA runs the transient motion cycle designed in Sec. IV to produce a forward scroll motion. D) The center FEA is extended slowly to click the scroll button, running the motion cycle designed in Sec V.

synthesis. For example, given a desired set of motion paths and/or static poses, generate the optimal (minimal) configuration of inlets, tubes, bellows, and valve placements. Finally, generating motion out of plane could significantly enhance the application space of viscous-driven actuators.

REFERENCES

[1] K. H. Petersen and R. F. Shepherd, "Fluid-driven intrinsically soft robots," in *Robotic Systems and Autonomous Platforms*. Elsevier, 2019, pp. 61–84.

[2] Y. Matia, G. H. Kaiser, R. F. Shepherd, A. D. Gat, N. Lazarus, and K. H. Petersen, "Harnessing nonuniform pressure distributions in soft robotic actuators," *Advanced Intelligent Systems*, vol. 5, no. 2, p. 2200330, 2023.

[3] D. Drotman, S. Jadhav, D. Sharp, C. Chan, and M. T. Tolley, "Electronics-free pneumatic circuits for controlling soft-legged robots," *Science Robotics*, vol. 6, no. 51, p. eaay2627, 2021.

[4] N. Vasios, A. J. Gross, S. Soifer, J. T. Overvelde, and K. Bertoldi, "Harnessing viscous flow to simplify the actuation of fluidic soft robots," *Soft robotics*, vol. 7, no. 1, pp. 1–9, 2020.

[5] R. F. Shepherd, F. Ilievski, W. Choi, S. A. Morin, A. A. Stokes, A. D. Mazzeo, X. Chen, M. Wang, and G. M. Whitesides, "Multigait soft robot," *Proceedings of the national academy of sciences*, vol. 108, no. 51, pp. 20 400–20 403, 2011.

[6] C. A. Aubin, R. H. Heisser, O. Peretz, J. Timko, J. Lo, E. F. Helbling, S. Sobhani, A. D. Gat, and R. F. Shepherd, "Powerful, soft combustion actuators for insect-scale robots," *Science*, vol. 381, no. 6663, pp. 1212–1217, 2023.

[7] M. T. Tolley, R. F. Shepherd, M. Karpelson, N. W. Bartlett, K. C. Galloway, M. Wehner, R. Nunes, G. M. Whitesides, and R. J. Wood, "An untethered jumping soft robot," in *2014 IEEE/RSJ International Conference on Intelligent Robots and Systems*. IEEE, 2014, pp. 561–566.

[8] C. C. Futran, S. Ceron, B. C. Mac Murray, R. F. Shepherd, and K. H. Petersen, "Leveraging fluid resistance in soft robots," in *2018 IEEE International Conference on Soft Robotics (RoboSoft)*. IEEE, 2018, pp. 473–478.

[9] L. Salem, B. Gamus, Y. Or, and A. D. Gat, "Leveraging viscous peeling to create and activate soft actuators and microfluidic devices," *Soft Robotics*, vol. 7, no. 1, pp. 76–84, 2020.

[10] Y. Matia, T. Elimelech, and A. D. Gat, "Leveraging internal viscous flow to extend the capabilities of beam-shaped soft robotic actuators," *Soft robotics*, vol. 4, no. 2, pp. 126–134, 2017.